

Distinguishing Various Models of the 125 GeV Boson in Vector Boson Fusion

Jung Chang¹, Kingman Cheung^{1,2}, Po-Yan Tseng¹, and Tzu-Chiang Yuan³

¹ *Department of Physics, National Tsing Hua University, Hsinchu 300, Taiwan*

² *Division of Quantum Phases and Devices, School of Physics,
Konkuk University, Seoul 143-701, Republic of Korea*

³ *Institute of Physics, Academia Sinica, Nangang, Taipei 11529, Taiwan*

(Dated: September 4, 2024)

Abstract

The hint of a new particle around 125 GeV at the LHC through the decay modes of diphoton and a number of others may point to quite a number of possibilities. While at the LHC the dominant production mechanism for the Higgs boson of the standard model and some other extensions is via the gluon fusion process, the alternative vector boson fusion is more sensitive to electroweak symmetry breaking through the gauge-Higgs couplings and therefore can be used to probe for models beyond the standard model. In this work, using the well known dijet-tagging technique to single out the vector boson fusion mechanism, we investigate its capability to discriminate a number of models that have been suggested to give an enhanced inclusive diphoton production rate, including the standard model Higgs boson, fermiophobic Higgs boson, Randall-Sundrum radion, inert-Higgs-doublet model, two-Higgs-doublet model, and the MSSM.

PACS numbers: 14.80.Bn.,14.80.Da,14.80.Ec

I. INTRODUCTION

At the end of 2011, both the ATLAS [1] and CMS [2] experiments at the Large Hadron Collider (LHC) have seen some excess of events of a possible Higgs candidate in the decays of $h \rightarrow \gamma\gamma$, $h \rightarrow WW^* \rightarrow \ell\nu\ell\nu$ and $h \rightarrow ZZ^* \rightarrow 4\ell$ channels. If one scrutinizes more closely these channels, one may notice that the excessive channels exhibit some correlations, even though it is still too early to say anything concrete. The Higgs boson hunt is now heating up again in 2012 as LHC is slightly upgraded to run at 8 TeV.

Further updates from both CMS and ATLAS were announced on July 4, 2012 [3]. The diphoton production rate is about a factor of 1.5 – 2 higher than that of the standard model (SM) Higgs boson, while the ZZ^* and WW^* rates are consistent with the SM Higgs boson within uncertainties. Nevertheless, the observed rates are consistent with either the SM Higgs boson or some other Higgs models.

The $H \rightarrow \gamma\gamma$ events collected by CMS and ATLAS can be divided into two categories: inclusive $\gamma\gamma X$ and exclusive $\gamma\gamma jj$ (though both experiments have more refined sub-divisions among various classes of events.) Presumably, the inclusive $\gamma\gamma X$ events include all production channels such as gluon fusion, vector-boson fusion, associated production, etc, among which gluon fusion dominates for production of the SM Higgs boson and most of the models considered in this work, except for the fermiophobic Higgs boson. On the other hand, exclusive $\gamma\gamma jj$ events mainly come from vector-boson fusion and associated production, which can be further disentangled by jet-tagging techniques. The vector-boson fusion produces energetic forward jets while associated production produces jets with $m_{jj} \approx m_W$ to m_Z . The current evidence of the Higgs boson in the diphoton channel comes mainly from inclusive $\gamma\gamma X$ events, simply because the inclusive event rate is much higher than the exclusive $\gamma\gamma jj$ event rate.

The main goal of this work is to test a number of models, which have been proposed to explain the excess in the inclusive Higgs diphoton events (the current evidence), using the exclusive $\gamma\gamma jj$ channel in vector-boson fusion (VBF). The exclusive VBF events with $\gamma\gamma jj$ in the final state are selected using the forward jet-tagging techniques which will be explained shortly. We will first choose the parameter-space region of each model that can account for the excess in the *inclusive* diphoton rate, and then in that region of parameter space we calculate the *exclusive* $jj\gamma\gamma$ VBF production rates. We found that the exclusive

$\gamma\gamma jj$ production rate in VBF channel can help distinguishing a number of popular models. This is the main result of our study.

We summarize a number of models that have been used to account for the excess in the inclusive $\gamma\gamma X$ data as follows.

1. The SM Higgs boson is still believed to be the most desirable candidate. It is still consistent with the data within uncertainty.
2. The lighter Higgs boson of the minimal supersymmetric standard model (MSSM) can acquire a large radiative correction from the top-stop sector to achieve a mass of 125 GeV, though it has been shown rather difficult to achieve an enhanced diphoton rate [4, 5]. However, it is possible when one of the staus is light enough, just above the LEP limit, and so the diphoton branching ratio is enhanced.
3. One of CP-even Higgs bosons in the next-to-minimal supersymmetric standard model (NMSSM) can account for the observed 125 GeV boson with an enhanced diphoton rate [6]. It could be the lightest or the second lightest one. The $U(1)$ -extended MSSM (UMSSM) is also possible to account for the observed boson [7]. The analyses for these extended MSSM models are much more involved and deserve dedicated studies. We shall not pursue them in this work.
4. The lighter CP-even Higgs boson of the two-Higgs-doublet model (2HDM) [8], which has enough free parameters in the model that allows one to achieve a large branching ratio into $\gamma\gamma$.
5. In the fermiophobic (FP) Higgs boson model, the Higgs boson is only responsible to generate the masses to W and Z bosons while the fermion masses are generated by some other means. Since the FP Higgs boson does not couple to the quarks, it cannot be produced via gluon fusion at hadronic colliders, but only through the vector boson fusion (VBF) and the associated production with a vector boson. Nevertheless, the FP Higgs boson lighter than 130 GeV has a much larger branching ratio into diphoton, such that it can still account for the observed inclusive diphoton rate at the LHC [9].
6. In Ref. [10], it was pointed out that the Randall-Sundrum (RS) radion, with enhanced couplings to gg and $\gamma\gamma$ due to trace anomaly, can explain the excess in the inclusive

diphoton production rate and suppressed WW and ZZ rates, which provides the most economical alternative solution to explain the observed data.

7. The inert-Higgs-doublet model (IHDM) [11], which is a special case of 2HDM, in which one of the doublets entirely decouples from the leptons, quarks, and gauge bosons while the other one takes on the role of the SM Higgs doublet. The production rate of the Higgs boson is the same as the SM one. However, the decay width of $h \rightarrow \gamma\gamma$ can be enhanced by the presence of the charged Higgs boson in the loop. It was shown [11] that the diphoton production rate can be enhanced by a factor of about $1 - 2$.
8. There may also be some possibilities that the SM-like Higgs boson first decays into two light scalar or pseudoscalar bosons, followed by subsequent decays into collimated pairs of photons, which appear as two photons in the final state [12]. We shall not pursue this kind of possibilities in this work.

On the other hand, instead of top-down approaches, it would also be useful to reversely determine the couplings and the nature of the observed 125 GeV particle by studying all the available data [13].

The disadvantage of gluon fusion is that it is not clear what particles and their masses running in the triangle loop. In some models, the contribution from a particular charged particle can increase or decrease the diphoton decay width, depending on the relative signs. For example, in the supersymmetric models, there are additional sfermions, charginos, charged Higgs bosons running in the loop, and therefore resulting in complicated dependence on the model parameters. On the other hand, the advantage of using WW fusion or associated production with a W or a Z boson is that the production diagram is clean and directly testing the couplings of hWW and hZZ . Furthermore, the WW fusion has a cross section at least a factor of 2 larger than the associated production. We therefore focus on WW fusion in this work. The WW fusion can be extracted by the presence of two energetic forward jets. We can impose selection cuts to select jets in forward rapidity and high energy region [14, 15]. By combining the production rates in the inclusive $\gamma\gamma X$ and exclusive $\gamma\gamma jj$ channels, one can obtain useful information about the nature of the 125 GeV new particle recently observed at the LHC.

In this work, we calculate the event rates in the WW fusion channel for a number of models that have been used to interpret the current LHC data of the 125 GeV ‘‘Higgs

boson". The theoretical cleanliness of WW fusion has been explained in the last paragraph. We believe that the WW fusion channel can help tremendously to discriminate various models. The organization of this paper is as follows. We briefly highlight a number of models in the next section, and the WW fusion and selection cuts in Sec. III. We give the decay branching ratios in Sec. IV and production rates in Sec. V. We conclude in Sec. VI.

II. MODELS

A. Standard Model Higgs Boson

The SM Higgs boson is still the most favorable candidate to interpret the observed boson, though the experimental data showed slightly excess in inclusive $\gamma\gamma X$ events over the prediction of the SM Higgs boson [3]. Production of the SM Higgs boson is dominated by gluon fusion, which is an order of magnitude larger than the next important mechanism – VBF.

B. Two-Higgs-Doublet Model (2HDM)

There are two Higgs doublets instead of just one in the 2HDM. In order to avoid dangerous tree level flavor-changing neutral currents, the popular 2HDMs are imposed a discrete symmetry. In the type I, all of the fermions couple to a single Higgs doublet, and do not couple to the second doublet; while in the type II, one doublet couples only to down-type quarks and another doublet couples to the up-type quarks. In this work, we focus on the type II, which has the same Higgs sector as the MSSM. The Higgs sector consists of two Higgs doublets

$$H_u = \begin{pmatrix} H_u^+ \\ H_u^0 \end{pmatrix}, \quad H_d = \begin{pmatrix} H_d^+ \\ H_d^0 \end{pmatrix},$$

where the subscripts u, d denote the right-handed quark singlet field that the Higgs doublet couples to. The electroweak symmetry is broken when the Higgs doublet fields develop the following VEVs:

$$\langle H_u \rangle = \begin{pmatrix} 0 \\ v_u \end{pmatrix}, \quad \langle H_d \rangle = \begin{pmatrix} 0 \\ v_d \end{pmatrix}.$$

Physically, there are two CP-even, one CP-odd, and a pair of charged Higgs bosons after electroweak symmetry breaking (EWSB), and the W and Z bosons as well as the SM fermions, except for neutrinos, acquire masses. The Yukawa couplings and masses for fermions can be obtained from the following Yukawa interactions after EWSB

$$\mathcal{L}_{\text{Yuk}} = -y_u \overline{Q}_L u_R \tilde{H}_u - y_d \overline{Q}_L d_R H_d + \text{h.c.}$$

where $\tilde{H}_u = i\tau_2 H_u^*$. The parameters of the model in the CP-conserving case include

$$m_h, m_H, m_A, m_{H^\pm}, \tan \beta \equiv \frac{v_u}{v_d}, \alpha$$

where α is the mixing angle between the two CP-even Higgs bosons. There are enough free parameters in the Higgs potential such that all the above parameters are free inputs to the model, in contrast to the MSSM where the Higgs potential is highly restricted by supersymmetry in addition to gauge symmetry.

The couplings of the two lighter and heavier CP-even Higgs bosons h and H respectively and the CP-odd Higgs boson A to the top, bottom quarks, and taus are given by, with a common factor of $-igm_f/2m_W$ being suppressed,

	$t\bar{t}$	$b\bar{b}$	$\tau^- \tau^+$
h :	$\cos \alpha / \sin \beta$	$-\sin \alpha / \cos \beta$	$-\sin \alpha / \cos \beta$
H :	$\sin \alpha / \sin \beta$	$\cos \alpha / \cos \beta$	$\cos \alpha / \cos \beta$
A :	$-i \cot \beta \gamma_5$	$-i \tan \beta \gamma_5$	$-i \tan \beta \gamma_5$

while the charged Higgs H^- couples to t and \bar{b} via

$$\bar{b}tH^- : \quad \frac{ig}{2\sqrt{2}m_W} [m_t \cot \beta (1 + \gamma_5) + m_b \tan \beta (1 - \gamma_5)] .$$

Other relevant couplings in WW fusion are those to gauge bosons are given by,

$$\begin{aligned} hW^+W^- : & \quad ig m_W \sin(\beta - \alpha) g^{\mu\nu} \\ hZZ : & \quad ig m_Z \frac{\sin(\beta - \alpha)}{\cos \theta_W} g^{\mu\nu} . \end{aligned}$$

Dominant production of the light CP-even Higgs boson h at the LHC is via gluon fusion, similar to the SM Higgs boson with the top quark running in the loop; however, in the large $\tan \beta$ region the bottom-quark contribution can also be substantial. Since the bottom-Yukawa coupling can be substantially enhanced, the gluon fusion cross section can be larger

than the SM. On the other hand, since the couplings of the h to the WW and ZZ are simply the SM values multiplied by $\sin(\alpha - \beta)$, WW fusion cross sections are in general smaller than the SM.

The decay into two photons is somewhat more complicated than the SM. Besides the couplings hWW , $ht\bar{t}$, and $hb\bar{b}$ are different, there are also the charged Higgs bosons running in the loop. The charged Higgs boson couples to the light CP-even Higgs with the coupling [4]

$$\lambda_{hH^+H^-} = \frac{m_h^2 - \lambda_5 v^2}{m_W^2} \cos(\beta + \alpha) + \frac{2m_{H^\pm}^2 - m_h^2}{2m_W^2} \sin(2\beta) \sin(\beta - \alpha) . \quad (1)$$

However, the $b \rightarrow s\gamma$ and B meson mixing constraints require the charged Higgs boson mass $m_{H^\pm} > 500$ GeV for intermediate to large values of $\tan\beta$ [16]. We will choose $m_{H^\pm} = 500$ GeV in our analysis below.

The overall diphoton production rate $\sigma(gg \rightarrow h) \times B(h \rightarrow \gamma\gamma)$ in gluon fusion can easily vary between 0.5 – 2 of the SM prediction depending on parameters [8]. It was shown in Ref. [8] that the enhancement in branching ratio can be obtained roughly along $\sin\alpha$ near zero for all $\tan\beta$ in the type II model. We will choose parameter space points there to illustrate.

C. Supersymmetric Higgs boson: MSSM

In order to achieve a mass of 125 GeV for the lighter CP-even Higgs boson, a very large radiative correction is needed, which essentially comes from top-stop loop. The approximate formula for the lighter CP-even Higgs boson is given by [4]

$$m_h^2 \approx m_Z^2 \cos^2 2\beta + \frac{3m_t^4}{4\pi^2 v^2} \left[\frac{1}{2} X_t + t + \frac{1}{16\pi^2} \left(\frac{3m_t^2}{2v^2} - 32\pi\alpha_s \right) t (X_t + t) \right] \quad (2)$$

where

$$X_t = \frac{2(A_t - \mu \cot\beta)^2}{M_{\text{SUSY}}^2} \left(1 - \frac{(A_t - \mu \cot\beta)^2}{12M_{\text{SUSY}}^2} \right), \quad t = \frac{M_{\text{SUSY}}^2}{m_t^2} \quad (3)$$

and $M_{\text{SUSY}} \sim 1$ TeV is the SUSY scale. A large A_t is needed to generate a large correction. Here we follow the findings in Ref. [17] for the parameter space: we choose $m_{Q_3} = m_{U_3} = 850$ GeV, $A_t = 1.4$ TeV, $m_A = 1$ TeV, and $\tan\beta = 60$. A detailed analysis of the MSSM parameter space based on Bayesian statistical analysis in light of the new observation of the 125 GeV Higgs candidate is also presented recently in Ref. [18]. The reason behind such a large $\tan\beta$ is the stau contribution to the diphoton branching ratio explained below [4, 5].

In the production part via gluon fusion, the difference between the SM and supersymmetric models is that squarks also run in the triangle loop. As the experimental data have pushed the squark masses of the first two generations to be quite heavy but not the third generation (stop and sbottom) the change in production rates could be substantial, especially in large $\tan\beta$. On the other hand, the decay into diphoton is more involved in SUSY models. All charged particles, including squarks, sleptons, charginos, charged Higgs boson can flow in the triangle loop. With the present constraints from experiments, the production rate into diphoton (equal to production cross section times the branching ratio into diphoton) in the MSSM is shown to be very similar to the SM one and that the diphoton production rate can hardly be enhanced by more than a factor of 1.5 [4, 5].

The formulas for the decay of the Higgs boson into two photons as well as production via gluon fusion can be found in Ref. [19]. The couplings of the lighter CP-even Higgs boson to the WW or ZZ are given by the SM ones multiplied by $\sin(\alpha-\beta)$. Therefore, the production rate in the WW fusion is in general similar to or smaller than the SM prediction.

We look at the parameter space in which the diphoton production rate would be larger than the SM value in the MSSM. It was shown in Ref. [17] that diphoton production rate can be larger than the SM one if one pushes the stau to be very light, just above the LEP limit. In addition to the above mentioned soft parameters, the other parameters are m_{L_3} , m_{E_3} , and the μ . Without loss of generality we choose [17]

$$m_{L_3} = m_{e_3} = 200 - 450 \text{ GeV} \quad \text{and} \quad \mu = 200 - 1000 \text{ GeV} , \quad (4)$$

in which we can scan for the diphoton production rate $\sigma(gg \rightarrow h)B(h \rightarrow \gamma\gamma)$ to be larger than the SM rate. The region essentially gives a light stau, which can enhance the $B(h \rightarrow \gamma\gamma)$. We will scan the region according to Eq. (4) and require the mass of the lighter CP-even Higgs boson around 125 GeV and the diphoton production rate larger than the SM value. ¹

D. Fermiophobic Higgs

With the name ‘‘fermiophobic’’ (FP) the Higgs boson only couples to the vector bosons at tree level, though higher-loop corrections can induce small couplings to fermions. In this

¹ There is another possibility that the heavier CP-even Higgs boson can be at around 125 GeV and its diphoton production rates can be enhanced relative to the SM one [20]. We will not pursue this further in this work.

case, the Yukawa couplings and masses of fermions are generated by some other mechanisms, which are not of concern in this work.

The coupling strength of the FP Higgs boson to vector bosons is the same as that of the SM Higgs boson. We write the interactions as

$$\mathcal{L}_{\text{FP}} = -gm_W h_{\text{FP}} W_\mu^+ W^{-\mu} - \frac{gm_Z}{2 \cos \theta_W} h_{\text{FP}} Z_\mu Z^\mu . \quad (5)$$

Since the FP Higgs boson does not couple to quarks, it cannot be produced dominantly by gluon fusion at hadronic colliders, but only through the vector boson fusion and the associated production with a W/Z boson. The corresponding production cross sections are the same as the VBF of the SM Higgs boson. Nevertheless, the FP Higgs boson lighter than 130 GeV has a much larger branching ratio into diphoton, such that it can still account for the observed diphoton rate at the LHC [9]. There are two reasons: (i) the FP Higgs boson decay into fermions is highly suppressed with only the loop-induced couplings, and (ii) the decay into photons is via a loop of W boson without the negative interference from the top quark. Thus, the branching ratio into diphoton can be enhanced by more than an order of magnitude. Overall, the diphoton production rate at the LHC is comparable to the SM Higgs boson, as was used to account for the observed boson [9]. An earlier study of FP Higgs boson at the LHC can be found in Ref. [21]. There is basically no free parameters in this model.

E. The Radion

The RS model [22] used a warped 5D space-time, a slice of the symmetric space AdS_5 , to explain the gauge hierarchy problem. The extra dimension φ is a single S^1/Z_2 orbifold with one hidden and one visible 3-brane localized at $\varphi = 0$ and π , respectively. It was pointed out by Goldberger and Wise [23] that the original RS model has a four-dimensional massless scalar (the modulus or radion) which does not have a potential and therefore the extra dimension cannot be stabilized. A stabilization mechanism was proposed in [23] by adding a bulk scalar field propagating in the background solution which can generate a potential to stabilize the modulus field. The minimum of the potential can be arranged to give the desired value of $kr_c \sim 12$ to solve the gauge hierarchy problem without extreme fine tuning of parameters. As a consequence, the lightest excitation mode of the modulus field is the

radion, which has a mass of the order of 100 GeV to a TeV, and the strength of its coupling to the SM fields is of the order of $O(1/\text{TeV})$ [24]. Phenomenology of the stabilized radion and its effects on the background geometry were studied in [25].

The interactions of the stabilized modulus (radion) ϕ with the SM particles on the visible brane are completely determined by 4-dimensional general covariance. Thus the radion Lagrangian is given by

$$\mathcal{L}_{\text{radion}} = \frac{\phi}{\Lambda_\phi} T_\mu^\mu(\text{SM}) , \quad (6)$$

where $\Lambda_\phi = \langle \phi \rangle$ is of the order of TeV and T_μ^μ is the trace of the SM energy-momentum stress tensor, which has the following lowest order terms

$$T_\mu^\mu(\text{SM}) = -2m_W^2 W_\mu^+ W^{-\mu} - m_Z^2 Z_\mu Z^\mu + \sum_f m_f \bar{f} f + (2m_h^2 h^2 - \partial_\mu h \partial^\mu h) + \dots . \quad (7)$$

The coupling of the radion to a pair of gluons (photons) is induced at one loop level, with the dominated contributions coming from the heavy top quark (top quark and W) as well as from the trace anomaly in QCD (QED). The expressions of the induced couplings can be found in Ref.[10]. Similar to the SM Higgs boson, the dominant production channel for the radion is via gg fusion, followed by VBF [26]. In addition, $gg \rightarrow \phi$ gets substantial enhancement from the trace anomaly. For the decay of the radion, it is dominated by the gg mode instead of $b\bar{b}$ at the low mass region, while its diphoton branching ratio is merely a fraction of the SM value of $h_{\text{SM}} \rightarrow \gamma\gamma$.

Overall, the diphoton production rate $\sigma(gg \rightarrow \phi) \times B(\phi \rightarrow \gamma\gamma)$ can be larger than the SM rate if the scale Λ_ϕ is small enough, and as long as it is consistent with the search for RS graviton. If we do not concern about naturalness, the scale Λ_ϕ can be as small as 0.8 TeV. In this work, We fix the scale Λ_ϕ to be 0.8 – 0.99 TeV, which can enhance the diphoton production rate in gluon fusion by a factor of 1.5 – 1.0 [10] relative to the SM rate. Note that the branching ratios of the radion is independent of Λ_ϕ .

F. Inert Higgs Doublet Model (IHDM)

IHDM is a special case of 2HDM, in which one of the doublets takes on the role of the SM Higgs doublet, while the other one is inert which means that it entirely decouples from the SM leptons, quarks, and gauge bosons. The model also has an additional Z_2 symmetry, for which all SM particles are even, except for the particle content of the second inert Higgs

doublet. The lightest Z_2 -odd particle of the second doublet can work as a candidate of dark matter. The Higgs sector consists of

$$H_1 = \begin{pmatrix} \phi_1^+ \\ \frac{v}{\sqrt{2}} + \frac{h+i\chi}{\sqrt{2}} \end{pmatrix}, \quad H_2 = \begin{pmatrix} \phi_2^+ \\ \frac{S+iA}{\sqrt{2}} \end{pmatrix}.$$

The electroweak symmetry is broken solely by one VEV:

$$\langle H_1 \rangle = \begin{pmatrix} 0 \\ \frac{v}{\sqrt{2}} \end{pmatrix}, \quad \langle H_2 \rangle = \begin{pmatrix} 0 \\ 0 \end{pmatrix}.$$

The Higgs potential is given by

$$V = \mu_1^2 |H_1|^2 + \mu_2^2 |H_2|^2 + \lambda_1 |H_1|^4 + \lambda_2 |H_2|^4 + \lambda_3 |H_1|^2 |H_2|^2 + \lambda_4 |H_1^\dagger H_2|^2 + \frac{\lambda_5}{2} [(H_1^\dagger H_2)^2 + \text{h.c.}]$$

Physically, there are 2 CP-even scalars (h, S), 1 CP-odd scalar (A), and a pair of charged Higgs (H^\pm). The h plays the role of the SM Higgs boson while the others are inert. A list of parameters of the model includes $m_h, m_S, m_A, m_{H^\pm}, \mu_2$, and λ_2 .

Production via gluon fusion and via WW fusion are the same as the SM Higgs boson. However, the decay into $\gamma\gamma$ receives additional contributions from the H^\pm running in the loop. If kinematically allowed the Higgs boson h can also decay into H^+H^- , AA , and SS . For simplicity and to achieve a large enough branching ratio into $\gamma\gamma$ we set the masses of S, A, H^+ to be above the threshold ($m_h/2$). In this model, the coupling between the charged Higgs boson and the SM Higgs boson h is given by

$$g_{hH^+H^-} = -i \frac{e}{m_W \sin \theta_W} (m_{H^\pm}^2 - \mu_2^2). \quad (8)$$

It is clear that from this equation the sign of the charged Higgs contribution to the triangular loop can be positive or negative, depending on the sizes of m_{H^+} and μ_2 . Thus, if we set $m_{H^+} = \mu_2$, the charged Higgs contribution vanishes and so the diphoton branching ratio becomes the same as the SM one.

It was shown in Ref. [11] that in gluon fusion the diphoton production rate is determined by the product of gluon-fusion cross section and the $\gamma\gamma$ branching ratio

$$\frac{\sigma(gg \rightarrow h) B(h \rightarrow \gamma\gamma)}{\sigma(gg \rightarrow h)_{\text{SM}} B(h \rightarrow \gamma\gamma)_{\text{SM}}} = \frac{B(h \rightarrow \gamma\gamma)}{B(h \rightarrow \gamma\gamma)_{\text{SM}}}, \quad (9)$$

which can be varied from about 0.5 to 2. The charged Higgs contribution to the diphoton branching ratio depends on the sizes of m_{H^\pm} and μ_2 . It was shown in Ref. [11] that when $m_{H^\pm}^2 < \mu_2^2$ the diphoton branching ratio is enhanced. Together with other theoretical constraints one can find the region to be $|\mu_2| \approx 100 - 200$ GeV and $m_{H^\pm} < |\mu_2|$.

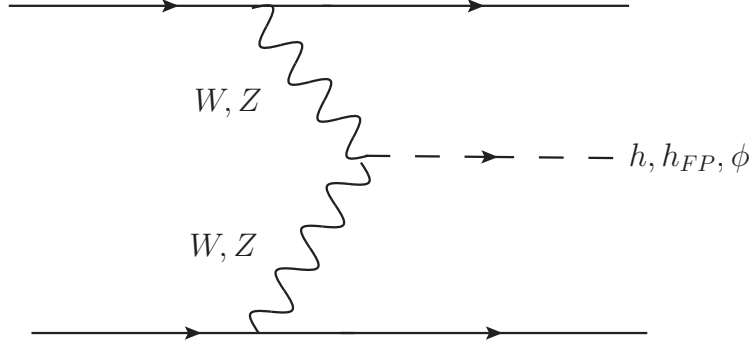


FIG. 1. A Feynman diagram showing the vector boson fusion into SM Higgs, FP Higgs or radion.

III. VECTOR BOSON FUSION (VBF)

The most distinguished feature of VBF at hadronic colliders is the appearance of two energetic forward jets separated by a large $\Delta R = \sqrt{(\Delta\eta)^2 + (\Delta\phi)^2}$, where η is the pseudo-rapidity and ϕ is the azimuth angle. The Feynman diagram is shown in Fig. 1. Each of the initial quarks radiates a W/Z boson, which further annihilates into the Higgs boson or some other particles under consideration. The unique feature of this process is that the W/Z bosons participating in the fusion process is close to on-shell [27], and whether the W/Z is longitudinal or transverse the scattered quark is very energetic carrying almost all the energy of the incoming quark and very forward [14, 15]. This fact justifies the use of effective W approximation in all calculations for VBF in the early days. Based on this feature we impose the following experimental cuts in selecting the dijet events coming dominantly from the VBF:

$$E_{T_j} > 30 \text{ GeV}, \quad |\eta_j| < 4.7, \quad \Delta R_{jj} > 3.5, \quad (10)$$

and

$$\begin{aligned} (\text{Ejcut}) \quad E_{j_1} > 500 \text{ GeV} \quad \text{or} \\ (\text{Mjjcut}) \quad M_{jj} > 350 \text{ GeV}, \end{aligned} \quad (11)$$

where the subscript “1” denotes the most energetic jet. In the cut of Eq. (11), we choose either the energy of the most energetic jet $E_{j_1} > 500 \text{ GeV}$ or the invariant mass of the jet pair $M_{jj} > 350 \text{ GeV}$. This set of cuts is similar to that used by CMS [28] and ATLAS [29] in their searches for FP Higgs boson.

The vector boson fusion is well-known that it allows to probe the direct coupling between

the vector bosons and the Higgs boson or other particles under consideration. This is in contrast to the gg fusion, because any colored particles can flow in the triangular loop and affect the production rate. For example, in MSSM all squarks can circulate inside the loop.

IV. DECAY BRANCHING RATIOS

Since the decay branching ratios for the SM Higgs boson, fermiophobic Higgs boson, and some benchmark points of the MSSM are publicly available, we simply use the listed values in literature [30]. For the other models (radion, IHDM, 2HDM) we calculate the branching ratios using exactly the same set of input parameters as the available models, so that a fair comparison is possible. We employ the full NLO QCD corrections for the decays of $h \rightarrow f\bar{f}$ and $h \rightarrow gg$ [31], and including offshellness in the decays $h \rightarrow W^*W^*$ and $h \rightarrow Z^*Z^*$, with the following b and c quark pole masses:

$$m_b^{\text{pole}} = 4.49 \text{ GeV}, \quad m_c^{\text{pole}} = 1.42 \text{ GeV}. \quad (12)$$

Here we list the decay branching ratio into $\gamma\gamma$ for the SM Higgs boson, fermiophobic Higgs boson, and the radion of mass 125 GeV in Table I. For the SM Higgs boson the decay into $\gamma\gamma$ goes through a triangle loop of W boson and top quark, between which they interfere destructively. The SM Higgs diphoton branching ratio is about 2.3×10^{-3} . This is very different for the FP Higgs boson, which allows only the W boson flowing in the loop. Thus, the branching ratio of a FP Higgs boson into diphoton can be an order of magnitude larger than that of the SM Higgs boson, and also because it does not decay into fermions. That is the reason why it can account for the observed 125 Higgs boson at the LHC, even though its gluon fusion production cross section is very small. The case of the radion is opposite to the FP Higgs. The diphoton branching ratio of the radion is a few times smaller than that of the SM, while its production rate via gg fusion is substantially enhanced.

We list the branching ratio into $\gamma\gamma$ for the Higgs boson in the IHDM for a number of choices of parameters of the model in Table II, such that the diphoton branching ratio is enhanced relative to the SM one: $|\mu_2| \approx 100\text{--}200 \text{ GeV}$ and $m_{H^\pm} < |\mu_2|$. The factors affecting the partial width into $\gamma\gamma$ are the charged Higgs boson mass and the coupling $g_{hH^+H^-}$. The charged Higgs loop contribution can interfere either constructively or destructively with the SM contributions. Another factor that would affect the branching ratio into $\gamma\gamma$ is whether

the thresholds into SS , AA , or H^+H^- are open. However, for our choices for m_S , m_{H^+} and m_A these decays would not be allowed. The diphoton branching ratio can be made similar to the SM one or enhanced by a few times.

We also list the branching ratio into $\gamma\gamma$ for the light CP-even Higgs boson in the 2HDM for a number of choices of parameters of the model in Table III, such that the enhancement in branching ratio can be achieved roughly along $\sin\alpha \approx 0$. Similar to IHDM, the main factors affecting the partial width into $\gamma\gamma$ are the charged Higgs boson mass and the coupling $g_{hH^+H^-}$. The branching ratio, on the other hand, also depends on other parameters such as $\tan\beta$ and $\sin\alpha$ as exhibited in the hWW and $ht\bar{t}$ couplings. Along $\sin\alpha \approx 0$, the factor $\cos\alpha \approx 1$ and the factor $\sin(\beta - \alpha) \approx 1$ for large $\tan\beta$, and thus the couplings hWW and $ht\bar{t}$ are close to their SM values. On the other hand, along $\sin\alpha = -1$ for large $\tan\beta$, the hWW coupling proportional to $\sin(\beta - \alpha)$ is only about $1/\tan\beta$. That is the reason why its branching ratio into $\gamma\gamma$ is very small. In Table III, we also list the values of $\sin^2(\alpha - \beta) \times B(h \rightarrow \gamma\gamma)$, which is directly proportional to the production rate of diphoton in VBF.

In the MSSM, we choose the region where the lighter CP-even Higgs boson is around 125 GeV (123 – 128 GeV) and the diphoton production rate $\sigma(gg \rightarrow h)B(h \rightarrow \gamma\gamma)$ is equal to or larger than the SM value. As explained above the stop sector must be heavy in order to achieve a mass of 125 GeV for the lighter CP-even Higgs boson. We follow closely the analysis in Ref. [17]. First, we fix the $m_{Q_3} = m_{U_3} = 850$ GeV and $A_t = 1.4$ TeV with $\tan\beta = 60$ and $m_A = 1$ TeV. Second, we vary $m_{E_3} = m_{L_3}$ and μ to achieve a light stau so as to enhance the diphoton production rate, according to Eq. (4). We used the FeynHiggs [32] to evaluate the branching ratio $B(h \rightarrow \gamma\gamma)$ and the diphoton production rate $\sigma(gg \rightarrow h)B(h \rightarrow \gamma\gamma)$ relative to the SM values. We show in Fig. 2 the region in the plane of $(m_{E_3} = m_{L_3}, \mu)$ that the $m_h = 123 - 128$ GeV and the ratio $\sigma(gg \rightarrow h)B(h \rightarrow \gamma\gamma)/\sigma(gg \rightarrow h_{\text{SM}})B(h_{\text{SM}} \rightarrow \gamma\gamma)$ is larger than 1. We also show the branching ratios into $\gamma\gamma$ for the lighter CP-even Higgs boson and the inclusive diphoton production rate for a few selective points of MSSM in Table IV.

V. PRODUCTION RATES IN VECTOR BOSON FUSION

We calculate the VBF cross sections for $pp \rightarrow jjh$ for various models under consideration. We impose the selection cuts for energetic forward jets as in Eqs. (10) and (11). We let the

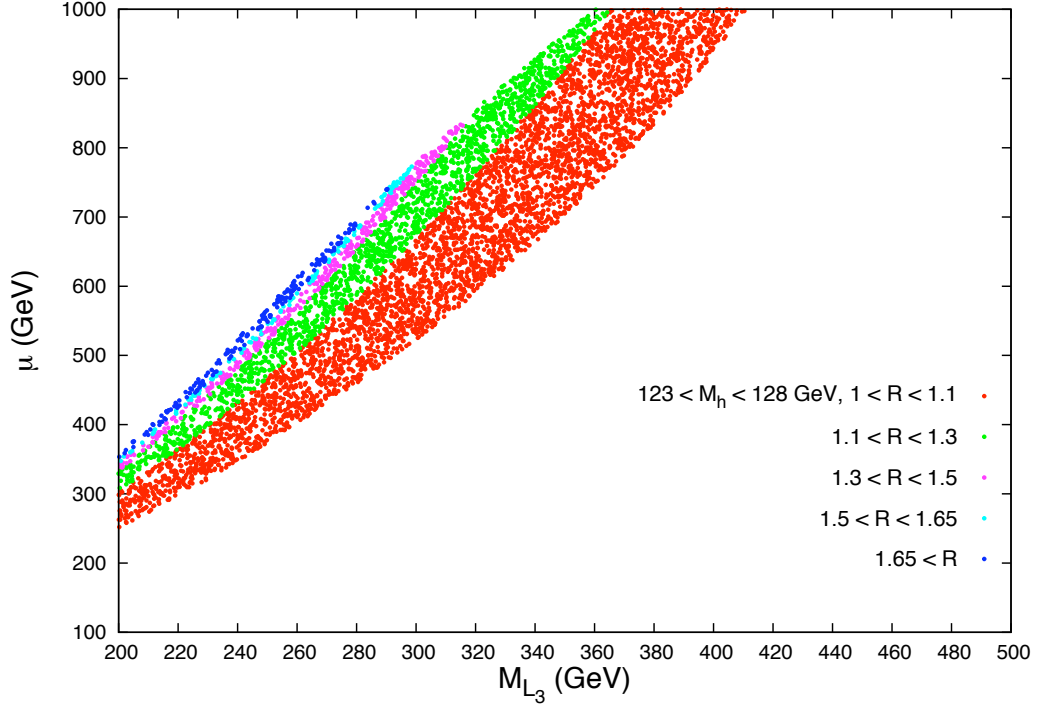


FIG. 2. The parameter space region where $m_h = 123 - 128$ GeV and $R = \sigma(gg \rightarrow h)B(h \rightarrow \gamma\gamma)/\sigma(gg \rightarrow h_{\text{SM}})B(h_{\text{SM}} \rightarrow \gamma\gamma)$ is larger than 1. The other fixed parameters are $m_{Q_3} = m_{U_3} = 850$ GeV, $A_t = 1.4$ TeV, $\tan\beta = 60$ and $m_A = 1$ TeV.

Higgs boson decay into $\gamma\gamma$, and impose the following cuts on the photons:

$$E_{T_\gamma} > 30 \text{ GeV}, \quad |\eta_\gamma| < 2.5, \quad |m_{\gamma\gamma} - m_h| < 3.5 \text{ GeV}. \quad (13)$$

In the following, we present numerical results in both parton level and detector-simulation level by employing the PYTHIA-PGS (PYTHIA v6.420, PGS4(090401)) package inside MADGRAPH [33].

A. Parton-level

We employ MADGRAPH [33] to calculate the production cross sections for $pp \rightarrow jjh \rightarrow jj\gamma\gamma$ and implementing the selection cuts for the forward jets and the diphoton. The production rates of diphoton for various models are then obtained by multiplying the corresponding

diphoton branching ratios.² The numerical results for LHC-7, LHC-8, and LHC-14 are listed in Table V for the SM, FP and radion, in Table VI for IHDM, in Table VII for 2HDM, and in Table VIII for the MSSM.

B. PGS Simulations

We use PYTHIA [34] for parton showering and hadronization. During the parton showering we turn on the initial and final state QED and QCD radiations (ISR and FSR), and fragmentation/hadronization according to the Lund model. We use PGS [35] for detector-simulation with the most general settings for the LHC. Electromagnetic and hadronic calorimeter resolutions are set at $0.2/\sqrt{E}$ and $0.8/\sqrt{E}$, respectively. We use the cone algorithm for jet finding with a cone size of $\Delta R = 0.5$, Sagitta resolution of $13 \mu\text{m}$ ($\delta p_T/p_T = 1.04 \times 10^{-4}$), track-finding efficiency of 0.98, and minimum track p_T of 1 GeV. More details can be found in Refs. [33, 35].

The numerical results for LHC-7, LHC-8, and LHC-14 after the PGS detector-simulation are listed in Table IX for the SM, FP and radion, in Table X for IHDM, in Table XI for the 2HDM, and in Table XII for MSSM.

A useful quantity that experimenters like to use is the production rate relative to the SM one

$$\frac{\sigma(pp \rightarrow jjX) \times B(X \rightarrow \gamma\gamma)}{\sigma(pp \rightarrow jjh_{\text{SM}}) \times B(h_{\text{SM}} \rightarrow \gamma\gamma)}, \quad (14)$$

where X stands for the SM Higgs or any other Higgs-like candidate in various models that we are studying in this work. We found that this ratio is quite robust against various cuts (M_{jcut} or E_{cut} as in Eq. (11)) and against the energy of the collision.

In the upper panel of Fig. 3, we first show the ratio for the *inclusive* diphoton production rate $\frac{\sigma(X) \times B(X \rightarrow \gamma\gamma)}{\sigma(h_{\text{SM}}) \times B(h_{\text{SM}} \rightarrow \gamma\gamma)}$ of each model, which is dominated by gluon fusion, except for the FP Higgs boson. The parameter space of each model is chosen such that this inclusive diphoton rate is equal to or larger than the SM rate except for the FP Higgs boson which has no free parameter. For the same parameter space, we show in the lower panel the ratio for the *exclusive* $jj\gamma\gamma$ production rate $\frac{\sigma(pp \rightarrow jjX) \times B(X \rightarrow \gamma\gamma)}{\sigma(pp \rightarrow jjh_{\text{SM}}) \times B(h_{\text{SM}} \rightarrow \gamma\gamma)}$ for each model. The figure is valid for

² The version of MADGRAPH that we used did not implement the loop decay. Therefore, we first let the MADGRAPH decay the Higgs boson 100% into diphoton and impose the cuts on the photons. Then we multiply the branching ratio of $h \rightarrow \gamma\gamma$ to obtain the diphoton production rate.

LHC-7, LHC-8 and LHC-14, and for using either M_{jj} cut on both forward jets or E_{jcut} cut on the most energetic jet.

It is clear that the models can be employed to explain the excess in the inclusive diphoton rates in some parameter space region, but for the same region of parameter space the ratio of exclusive VBF production would be different among the models. The FP Higgs would be a number of times larger than the SM in the VBF channel, but the RS radion would give negligible exclusive VBF production. On the other hand, the IHDM, 2HDM, and the MSSM would give similar ratios in both inclusive and exclusive production. The 2HDM can give a somewhat smaller ratio in the exclusive VBF.

C. Background Discussion

The experimental details for VBF in the context of searching for the FP Higgs boson are given in Ref. [28]. The dominant backgrounds to $h \rightarrow \gamma\gamma$ consist of i) the irreducible background from the prompt diphoton production, and ii) the reducible backgrounds from $pp \rightarrow \gamma + j$ and $pp \rightarrow jj$, when one or more of the jets hadronize into (typically neutral) pions and deposit energy in the electromagnetic calorimeter. These reconstructed objects are generally referred to as fake photons. Isolation is a very useful tool to reject the non-prompt background coming from electromagnetic showers originating in jets, because these fake photons are often accompanied by single and multiple π^0 s.

The dijet tag, as defined in Eqs. (10) and (11), together with the Higgs boson decaying into diphoton selects a special class of events consisting of two photons and two forward energetic jets. A signal-to-background ratio of order 1 can be achieved [28]. The signal from $h \rightarrow \gamma\gamma$ will be identified as a sharp peak in the $m_{\gamma\gamma}$ distribution, where the background is in continuum. In Ref. [28], the background model is derived from data. In the new run at 8 TeV, we expect the same treatment is applied to the background. The estimation of significance of each signal is beyond the scope of the present paper.

VI. CONCLUSIONS

LHC is expected to confirm if there is a new particle at 125 GeV by the end of this year. The likelihood for a new discovery is rather high. Nevertheless, whether this new particle is

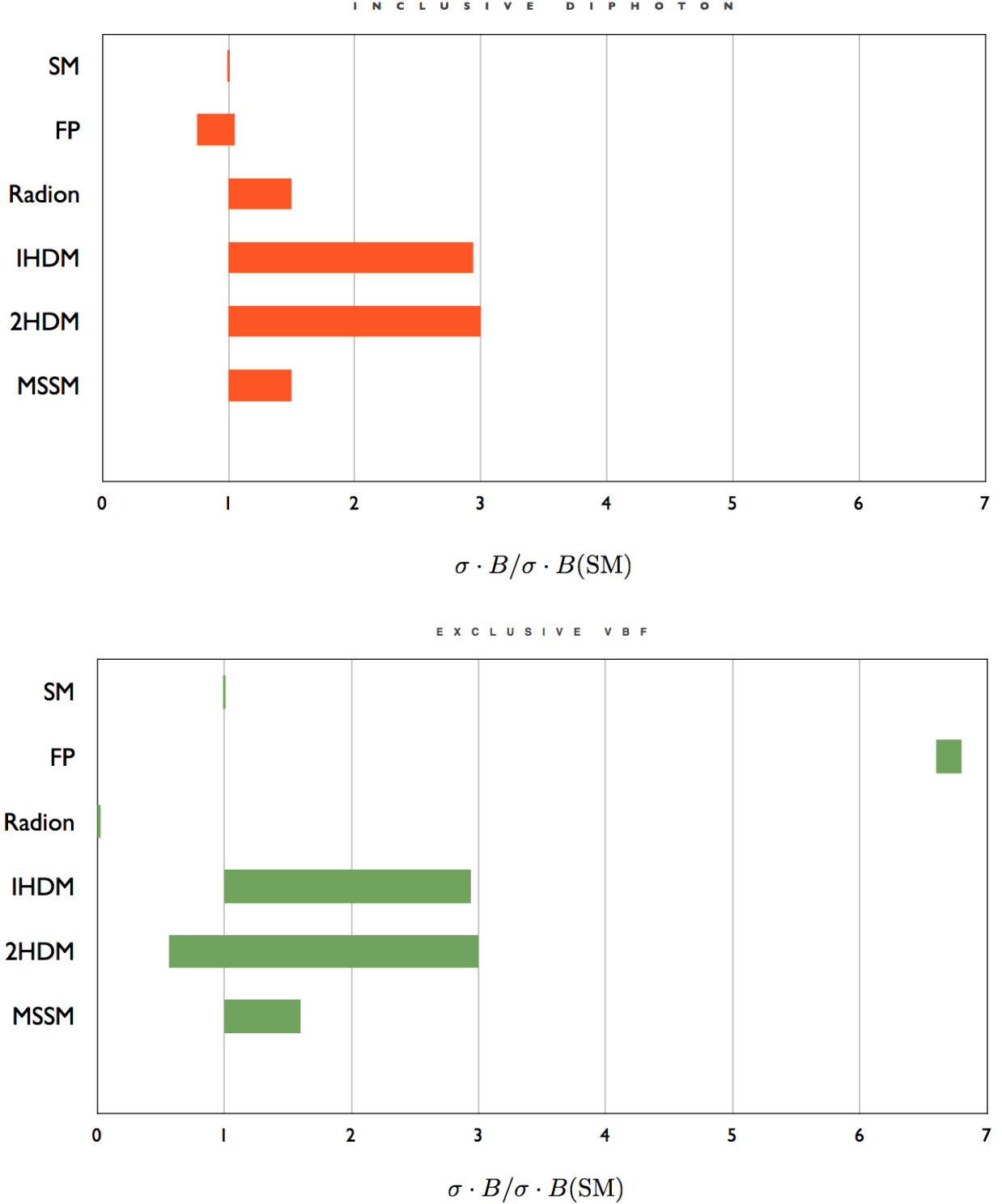


FIG. 3. *Upper:* the ratio of *inclusive* diphoton production rates $\frac{\sigma(X) \times B(X \rightarrow \gamma\gamma)}{\sigma(h_{\text{SM}}) \times B(h_{\text{SM}} \rightarrow \gamma\gamma)}$ for various models. The parameter space is chosen such that the ratio is equal to or larger than 1, except for the FP Higgs boson which has no free parameter. *Lower:* the ratio of the *exclusive* $jj\gamma\gamma$ production rate $\frac{\sigma(pp \rightarrow jjX) \times B(X \rightarrow \gamma\gamma)}{\sigma(pp \rightarrow jjh_{\text{SM}}) \times B(h_{\text{SM}} \rightarrow \gamma\gamma)}$ for each model in the corresponding parameter space.

the SM Higgs boson is not an easy question to answer.

In this work, the scenario of this 125 GeV particle produced by vector boson fusion, instead of gluon fusion as the dominant production mechanism for the standard model Higgs boson, is studied in details. By using the forward dijet tagging technique, one can single out the vector boson fusion mechanism. We studied a number of popular new physics models that have been employed to interpret the observed particle at 125 GeV, including fermiophobic Higgs boson, the Randall-Sundrum radion, inert-Higgs-doublet model, two-Higgs-doublet model, and the MSSM. Since the inclusive diphoton channel showed an excess over the SM predictions, we first selected the parameter space of each model that can give an inclusive diphoton rate larger than or equal to the SM rate. Then, we calculate the exclusive $jj\gamma\gamma$ diphoton production rate in VBF for that parameter space. The results are tabulated in Tables (V) - (VIII) at the parton level and in Tables (IX) - (XII) at the detector-simulation level.

If the diphoton mode excess seen at LHC-7 can be firmly established by the new LHC-8 data, it will be the utmost task to identify the nature of this particle. Perhaps, it is simply the SM Higgs boson with some level of statistical fluctuation, but it could also be the RS radion [10], fermiophobic Higgs boson [9], the light CP-even Higgs boson of the 2HDM [8], the Higgs boson of the IHDM [11], or one of the CP-even Higgs bosons in other extensions of the MSSM [6, 7], all of which can allow an enhancement to the $\gamma\gamma$ production rate. On the other hand, the vector boson fusion, as singled out by the dijet tag, provides an essential discriminator to differentiate various models. It is not hard by browsing through Tables (IX) and (XII) or Fig. 3 to conclude the following (here “excess” means excess over the SM Higgs boson prediction):

- If a similar rate is seen in inclusive production but a large excess is seen in the exclusive VBF production it would be a fermiophobic Higgs boson.
- If a similar rate or excess is seen in inclusive production but a negligible exclusive VBF production rate, it would be the RS radion.
- If moderate excess is seen in both inclusive production and exclusive VBF production, it could be the Higgs boson of the IHDM, 2HDM, or the MSSM. However, if the excess is over 60% it will pose severe challenge to the MSSM.

If the production rate of the diphoton mode at 125 GeV lines up with the SM prediction eventually, it is still premature to conclude this is coming from the SM Higgs boson. Other alternatives in MSSM, NMSSM, or other SUSY models can also be mimicking the SM Higgs boson, depending on the parameter space of the new physics model. In any case, once the signals at 125 GeV are confirmed further studies including all possible decay modes are to be taken into account in order to discriminate these many alternatives beyond the standard model.

Vector boson fusion is the next most important production mechanism that must be taken into account to fully identify the newly discovered particle.

ACKNOWLEDGMENT

This work was supported in part by the National Science Council of Taiwan under Grants No. 99-2112-M-007-005-MY3 and No. 101-2112-M-001-005-MY3 as well as the WCU program through the KOSEF funded by the MEST (R31-2008-000-10057-0). The hospitalities from the faculty and staff members received by TCY at both NCTS and KITPC are happily acknowledged.

-
- [1] G. Aad *et al.* [ATLAS Collaboration], Phys. Lett. B **710**, 49 (2012) [arXiv:1202.1408 [hep-ex]].
 - [2] S. Chatrchyan *et al.* [CMS Collaboration], Phys. Lett. B **710**, 26 (2012) [arXiv:1202.1488 [hep-ex]].
 - [3] G. Aad *et al.* [The ATLAS Collaboration], arXiv:1207.7214 [hep-ex]; S. Chatrchyan *et al.* [The CMS Collaboration], arXiv:1207.7235 [hep-ex].
 - [4] See for example, M. Carena, S. Gori, N. R. Shah and C. E. M. Wagner, JHEP **1203**, 014 (2012) [arXiv:1112.3336 [hep-ph]]; N. D. Christensen, T. Han and S. Su, arXiv:1203.3207 [hep-ph].
 - [5] P. Nath, private communication. P. Nath *et al.*, work in progress.
 - [6] U. Ellwanger, JHEP **1203**, 044 (2012) [arXiv:1112.3548 [hep-ph]]; J. F. Gunion, Y. Jiang and S. Kraml, Phys. Lett. B **710**, 454 (2012) [arXiv:1201.0982 [hep-ph]]; J. Cao, Z. Heng, J. M. Yang, Y. Zhang and J. Zhu, JHEP **1203**, 086 (2012) [arXiv:1202.5821 [hep-ph]]; U. Ellwanger and C. Hugonie, arXiv:1203.5048 [hep-ph].

- [7] C. -F. Chang, K. Cheung, Y. -C. Lin and T. -C. Yuan, JHEP **1206** 128 (2012), [arXiv:1202.0054 [hep-ph]].
- [8] P. M. Ferreira, R. Santos, M. Sher and J. P. Silva, Phys. Rev. D **85**, 077703 (2012) [arXiv:1112.3277 [hep-ph]]; G. Burdman, C. E. F. Haluch and R. D. Matheus, Phys. Rev. D **85**, 095016 (2012) [arXiv:1112.3961 [hep-ph]]; E. Cervero and J. -M. Gerard, Phys. Lett. B **712**, 255 (2012) [arXiv:1202.1973 [hep-ph]].
- [9] E. Gabrielli, B. Mele and M. Raidal, arXiv:1202.1796 [hep-ph]; E. L. Berger, Z. Sullivan and H. Zhang, arXiv:1203.6645 [hep-ph].
- [10] K. Cheung and T. -C. Yuan, Phys. Rev. Lett. **108**, 141602 (2012) [arXiv:1112.4146 [hep-ph]]; V. Barger, M. Ishida and W. -Y. Keung, Phys. Rev. Lett. **108**, 101802 (2012) [arXiv:1111.4473 [hep-ph]]; *ibid.* Phys. Rev. D **85**, 015024 (2012) [arXiv:1111.2580 [hep-ph]]; B. Grzadkowski, J. F. Gunion and M. Toharia, Phys. Lett. B **712**, 70 (2012) [arXiv:1202.5017 [hep-ph]]; Y. Tang, arXiv:1204.6145 [hep-ph]; S. Matsuzaki and K. Yamawaki, Phys. Rev. D **85**, 095020 (2012) [arXiv:1201.4722 [hep-ph]]; H. de Sandes and R. Rosenfeld, Phys. Rev. D **85**, 053003 (2012) [arXiv:1111.2006 [hep-ph]].
- [11] A. Arhrib, R. Benbrik and N. Gaur, Phys. Rev. D **85**, 095021 (2012) [arXiv:1201.2644 [hep-ph]].
- [12] P. Draper and D. McKeen, Phys. Rev. D **85**, 115023 (2012) [arXiv:1204.1061 [hep-ph]].
- [13] D. Carmi, A. Falkowski, E. Kuflik and T. Volansky, arXiv:1202.3144 [hep-ph]; A. Azatov, R. Contino and J. Galloway, JHEP **1204**, 127 (2012) [arXiv:1202.3415 [hep-ph]]; J. R. Espinosa, C. Grojean, M. Muhlleitner and M. Trott, JHEP **1205**, 097 (2012) [arXiv:1202.3697 [hep-ph]]; V. Barger, M. Ishida and W. -Y. Keung, Phys. Rev. Lett. **108**, 261801 (2012) [arXiv:1203.3456 [hep-ph]]; P. P. Giardino, K. Kannike, M. Raidal and A. Strumia, JHEP **1206**, 117 (2012) [arXiv:1203.4254 [hep-ph]]; J. Ellis and T. You, JHEP **1206**, 140 (2012) [arXiv:1204.0464 [hep-ph]]; A. Azatov, R. Contino, D. Del Re, J. Galloway, M. Grassi and S. Rahatlou, JHEP **1206**, 134 (2012) [arXiv:1204.4817 [hep-ph]]; M. Klute, R. Lafaye, T. Plehn, M. Rauch and D. Zerwas, arXiv:1205.2699 [hep-ph].
- [14] J. Bagger, V. D. Barger, K. -m. Cheung, J. F. Gunion, T. Han, G. A. Ladinsky, R. Rosenfeld and C. -P. Yuan, Phys. Rev. D **52**, 3878 (1995) [hep-ph/9504426].
- [15] D. L. Rainwater and D. Zeppenfeld, JHEP **9712**, 005 (1997) [hep-ph/9712271].
- [16] K. Cheung and O. C. W. Kong, Phys. Rev. D **68**, 053003 (2003) [hep-ph/0302111].

- [17] M. Carena, S. Gori, N. R. Shah, C. E. M. Wagner and L. -T. Wang, JHEP **1207**, 175 (2012) [arXiv:1205.5842 [hep-ph]].
- [18] S. Akula, P. Nath and G. Peim, arXiv:1207.1839 [hep-ph].
- [19] J. F. Gunion, H. E. Haber, G. L. Kane and S. Dawson, Front. Phys. **80**, 1 (2000).
- [20] K. Hagiwara, J. S. Lee and J. Nakamura, arXiv:1207.0802 [hep-ph].
- [21] A. G. Akeroyd, J. Phys. G **24**, 1983 (1998) [hep-ph/9803324].
- [22] L. Randall and R. Sundrum, Phys. Rev. Lett. **83**, 3370 (1999); *ibid.* **83**, 4690 (1999).
- [23] W. Goldberger and M. Wise, Phys. Rev. Lett. **83**, 4922 (1999).
- [24] W. Goldberger and M. Wise, Phys. Lett. **B475** 275 (2000).
- [25] C. Csáki, M. Graesser, L. Randall and J. Terning, Phys. Rev. D **62**, 045015 (2000); C. Csáki, M. L. Graesser and G. D. Kribs, Phys. Rev. D **63**, 065002 (2001) [hep-th/0008151].
- [26] K. -m. Cheung, Phys. Rev. D **63**, 056007 (2001) [hep-ph/0009232]; W. D. Goldberger, B. Grinstein and W. Skiba, Phys. Rev. Lett. **100**, 111802 (2008) [arXiv:0708.1463 [hep-ph]].
- [27] M. S. Chanowitz, Ann. Rev. Nucl. Part. Sci. **38**, 323 (1988).
- [28] CMS Collaboration, CMS-PAS-HIG-12-002.
- [29] ATLAS Collaboration, ATLAS-CONF-2012-13.
- [30] LHC Higgs Cross Section Working Group, S. Dittmaier, C. Mariotti, G. Passarino, and R. Tanaka (Eds.), *Handbook of LHC Higgs Cross Sections: 1. Inclusive Observables*, CERN-2011-002 (CERN, Geneva, 2011), arXiv:1101.0593 [hep-ph].
- [31] A. Djouadi, Phys. Rept. **457**, 1 (2008) [hep-ph/0503172].
- [32] M. Frank, T. Hahn, S. Heinemeyer, W. Hollik, H. Rzehak and G. Weiglein, JHEP **0702**, 047 (2007) [hep-ph/0611326].
- [33] MADGRAPH: J. Alwall, M. Herquet, F. Maltoni, O. Mattelaer and T. Stelzer, JHEP **1106**, 128 (2011) [arXiv:1106.0522 [hep-ph]].
- [34] T. Sjostrand, S. Mrenna and P. Z. Skands, Comput. Phys. Commun. **178**, 852 (2008) [arXiv:0710.3820 [hep-ph]].
- [35] The MG/ME Pythia-PGS package, J. Alwall and the CP3 development team.

TABLE I. Decay branching ratio $B(h \rightarrow \gamma\gamma)$ with $m_h = 125$ GeV for the SM Higgs boson h_{SM} , the fermiophobic Higgs boson h_{FP} , and the radion ϕ .

	$B(h \rightarrow \gamma\gamma)$
SM	$B(h_{\text{SM}} \rightarrow \gamma\gamma) = 2.3 \times 10^{-3}$
FP	$B(h_{\text{FP}} \rightarrow \gamma\gamma) = 1.5 \times 10^{-2}$
Radion	$B(\phi \rightarrow \gamma\gamma) = 0.57 \times 10^{-3}$

TABLE II. Decay branching ratio $B(h \rightarrow \gamma\gamma)$ with $m_h = 125$ GeV of the IHDM. We have set $m_S = 75$ GeV and chosen the points with $m_{H^\pm} \leq |\mu_2|$.

	μ_2 (GeV)	m_{H^\pm} (GeV)	$B(h \rightarrow \gamma\gamma)$
IHDM1	200	70	6.7×10^{-3}
IHDM2	200	100	3.3×10^{-3}
IHDM3	200	150	2.5×10^{-3}
IHDM4	200	200	2.3×10^{-3}
IHDM5	150	70	4.2×10^{-3}
IHDM6	150	100	2.7×10^{-3}
IHDM7	150	120	2.5×10^{-3}
IHDM8	150	150	2.3×10^{-3}
IHDM9	100	70	2.8×10^{-3}
IHDM10	100	90	2.4×10^{-3}
IHDM11	100	100	2.3×10^{-3}

TABLE III. Decay branching ratio $B(h \rightarrow \gamma\gamma)$ for the lighter CP-even Higgs boson in the 2HDM. We fix $m_h = 125$ GeV, $m_{H^\pm} = 500$ GeV, and $\lambda_5 = \frac{m_h^2}{v^2}$. With $m_{H^\pm} = 500$ GeV and λ_5 varies from 0 to 10, the $B(h \rightarrow \gamma\gamma)$ stays approximately the same. We have chosen parameter space points with $\sin \alpha \approx 0$ for a wide range of $\tan \beta$.

	$\sin \alpha$	$\tan \beta$	$B(h \rightarrow \gamma\gamma)$	$\sin^2(\alpha - \beta) \times B(h \rightarrow \gamma\gamma)$
2HDM1	0	1.5	3.8×10^{-3}	2.6×10^{-3}
2HDM2	0	5	6.5×10^{-3}	6.2×10^{-3}
2HDM3	0	10	6.8×10^{-3}	6.7×10^{-3}
2HDM4	0	20	6.9×10^{-3}	6.9×10^{-3}
2HDM5	0.1	1.5	3.0×10^{-3}	1.8×10^{-3}
2HDM6	0.1	5	4.0×10^{-3}	3.6×10^{-3}
2HDM7	0.1	9	2.4×10^{-3}	2.3×10^{-3}
2HDM8	-0.1	1	2.2×10^{-3}	1.3×10^{-3}
2HDM9	-0.1	5	4.4×10^{-3}	4.4×10^{-3}
2HDM10	-0.1	10	2.3×10^{-3}	2.3×10^{-3}

TABLE IV. The decay branching ratio $B(h \rightarrow \gamma\gamma)$ and the diphoton production rates $\sigma(gg \rightarrow h)B(h \rightarrow \gamma\gamma)$ relative to the SM values for some parameter space points in MSSM, chosen according to Eq. (4). Other parameters are $m_{Q_3} = m_{U_3} = 850$ GeV, $A_t = 1.4$ TeV, $\tan \beta = 60$, and $m_A = 1$ TeV. Mass parameters are given in GeV.

MSSM					
	$m_{L_3} = m_{E_3}$	μ	m_h	$B(h \rightarrow \gamma\gamma)$	$\frac{\sigma(gg \rightarrow h)B(h \rightarrow \gamma\gamma)}{\sigma(gg \rightarrow h_{\text{SM}})B(h_{\text{SM}} \rightarrow \gamma\gamma)}$
BP1	250	400	127.0	2.4×10^{-3}	1.02
BP2	250	500	126.2	2.9×10^{-3}	1.19
BP3	250	536	125.4	3.6×10^{-3}	1.45
BP4	300	536	126.8	2.4×10^{-3}	1.005
BP5	300	700	125.4	2.8×10^{-3}	1.15
BP6	300	763	123.7	3.4×10^{-3}	1.38
BP7	350	700	126.6	2.4×10^{-3}	0.999
BP8	350	800	125.8	2.5×10^{-3}	1.03
BP9	350	927	123.9	2.7×10^{-3}	1.11

TABLE V. Production rates (in fb) at parton level for $pp \rightarrow jjh \rightarrow jj\gamma\gamma$ for the SM, FP, and radion at the LHC-7 (LHC-8, LHC-14). Here $\sigma \cdot B$ denotes $\sigma(pp \rightarrow jjh) \times B(h \rightarrow \gamma\gamma)$. The dijet tag is given in Eqs. (10) and (11) (Ejcut or Mjjcut) and the photon cuts are in Eq. (13).

Model	$\sigma \cdot B$ (fb)		
	w/o cuts	w/ photon cuts and Ejcut	w/ photon cuts and Mjjcut
SM	2.66 (3.39, 8.54)	0.26 (0.38, 1.27)	0.60 (0.80, 2.20)
FP	17.94 (22.87, 57.67)	1.78 (2.54, 8.55)	4.03 (5.42, 14.83)
Radion	0.062 (0.080, 0.20)	0.0066 (0.0085, 0.030)	0.014 (0.019, 0.052)

TABLE VI. Production rates (in fb) at parton level for $pp \rightarrow jjh \rightarrow jj\gamma\gamma$ for the IHDM at the LHC-7 (LHC-8, LHC-14). Here $\sigma \cdot B$ denotes $\sigma(pp \rightarrow jjh) \times B(h \rightarrow \gamma\gamma)$. The dijet tag is given in Eqs. (10) and (11) (Ejcut or Mjjcut) and the photon cuts are in Eq. (13).

Model	$\sigma \cdot B$ (fb)		
	w/o cuts	w/ photon cuts and Ejcut	w/ photon cuts and Mjjcut
IHDM1	7.81 (9.96, 25.09)	0.76 (1.12, 3.73)	1.76 (2.35, 6.46)
IHDM2	3.85 (4.91, 12.36)	0.38 (0.55, 1.84)	0.87 (1.16, 3.18)
IHDM3	2.92 (3.72, 9.36)	0.28 (0.42, 1.39)	0.66 (0.88, 2.41)
IHDM4	2.68 (3.42, 8.61)	0.26 (0.38, 1.28)	0.61 (0.81, 2.22)
IHDM5	4.90 (6.24, 15.73)	0.48 (0.70, 2.34)	1.11 (1.47, 4.05)
IHDM6	3.15 (4.01, 10.11)	0.31 (0.45, 1.50)	0.71 (0.95, 2.61)
IHDM7	2.92 (3.72, 9.36)	0.29 (0.42, 1.39)	0.66 (0.88, 2.41)
IHDM8	2.68 (3.42, 8.61)	0.26 (0.38, 1.28)	0.61 (0.81, 2.22)
IHDM9	3.27 (4.16, 10.49)	0.32 (0.47, 1.56)	0.74 (0.98, 2.70)
IHDM10	2.80 (3.57, 8.99)	0.27 (0.40, 1.34)	0.63 (0.84, 2.3)
IHDM11	2.68 (3.42, 8.61)	0.26 (0.38, 1.28)	0.61 (0.81, 2.22)

TABLE VII. Production rates (in fb) at parton level for $pp \rightarrow jjh \rightarrow jj\gamma\gamma$ for the 2HDM at the LHC-7 (LHC-8, LHC-14). Here $\sigma \cdot B$ denotes $\sigma(pp \rightarrow jjh) \times B(h \rightarrow \gamma\gamma)$. The dijet tag is given in Eqs. (10) and (11) (Ejcut or Mjcut) and the photon cuts are in Eq. (13).

Model	$\sigma \cdot B$ (fb)		
	w/o cuts	w/ photon cuts and Ejcut	w/ photon cuts and Mjcut
2HDM1	2.48 (2.97, 7.00)	0.34 (0.43, 1.47)	0.74 (0.89, 2.61)
2HDM2	5.88 (7.05, 16.6)	0.82 (1.02, 3.49)	1.76 (2.10, 6.18)
2HDM3	6.34 (7.61, 17.9)	0.88 (1.10, 3.77)	1.89 (2.27, 6.67)
2HDM4	6.48 (7.78, 18.3)	0.90 (1.13, 3.85)	1.94 (2.32, 6.82)
2HDM5	1.71 (2.05, 4.83)	0.24 (0.30, 1.02)	0.51 (0.61, 1.80)
2HDM6	3.42 (4.10, 9.65)	0.47 (0.59, 2.03)	1.02 (1.22, 3.60)
2HDM7	2.14 (2.57, 6.04)	0.30 (0.37, 1.27)	0.64 (0.76, 2.25)
2HDM8	1.26 (1.51, 3.56)	0.17 (0.22, 0.75)	0.38 (0.45, 1.33)
2HDM9	4.10 (4.92, 11.6)	0.57 (0.71, 2.44)	1.23 (1.47, 4.32)
2HDM10	2.15 (2.58, 6.06)	0.30 (0.37, 1.28)	0.64 (0.77, 2.26)

TABLE VIII. Production rates (in fb) at parton level for $pp \rightarrow jjh \rightarrow jj\gamma\gamma$ for selected MSSM benchmark points at the LHC-7 (LHC-8, LHC-14). Here $\sigma \cdot B$ denotes $\sigma(pp \rightarrow jjh) \times B(h \rightarrow \gamma\gamma)$. The dijet tag is given in Eqs. (10) and (11) (Ejcut or Mjjcut) and the photon cuts are in Eq. (13).

MSSM BP	$\sigma \cdot B$ (fb)		
	w/o cuts	w/ photon cuts and Ejcut	w/ photon cuts and Mjjcut
BP1	2.83 (3.60, 9.18)	0.30 (0.42, 1.39)	0.66 (0.86, 2.51)
BP2	3.35 (4.25, 10.85)	0.36 (0.50, 1.64)	0.79 (1.02, 2.95)
BP3	4.15 (5.28, 13.41)	0.46 (0.63, 2.03)	0.99 (1.29, 3.63)
BP4	2.79 (3.56, 9.05)	0.30 (0.42, 1.41)	0.67 (0.86, 2.45)
BP5	3.27 (4.15, 10.56)	0.36 (0.50, 1.60)	0.78 (0.99, 2.87)
BP6	4.03 (5.01, 12.95)	0.43 (0.59, 1.88)	0.94 (1.19, 3.36)
BP7	2.78 (3.53, 9.03)	0.31 (0.42, 1.36)	0.66 (0.85, 2.47)
BP8	2.90 (3.69, 9.39)	0.31 (0.44, 1.43)	0.68 (0.89, 2.52)
BP9	3.22 (4.09, 10.38)	0.36 (0.49, 1.52)	0.75 (0.96, 2.76)

TABLE IX. Production rates (in fb) at detector-simulation level (after PGS) for $pp \rightarrow jjh \rightarrow jj\gamma\gamma$ for the SM, FP, and radion, at the LHC-7 (LHC-8, LHC-14). Here $\sigma \cdot B$ denotes $\sigma(pp \rightarrow jjh) \times B(h \rightarrow \gamma\gamma)$. The dijet tag is given in Eqs. (10) and (11) (Ejcut or Mjjcut) and the photon cuts are in Eq. (13).

Model	$\sigma \cdot B$ (fb)	
	w/ photon cuts and Ejcut	w/ photon cuts and Mjjcut
SM	0.15 (0.19, 0.61)	0.33 (0.41, 1.1)
FP	1.03 (1.27, 4.12)	2.24 (2.78, 7.35)
Radion	0.0038 (0.0047, 0.014)	0.0076 (0.0095, 0.026)

TABLE X. Production rates (in fb) at detector-simulation level (after PGS) for $pp \rightarrow jjh \rightarrow jj\gamma\gamma$ for the IHDM at the LHC-7 (LHC-8, LHC-14). Here $\sigma \cdot B$ denotes $\sigma(pp \rightarrow jjh) \times B(h \rightarrow \gamma\gamma)$. The dijet tag is given in Eqs. (10) and (11) (Ejcut or Mjjcut) and the photon cuts are in Eq. (13).

Model	$\sigma \cdot B$ (fb)	
	w/ photon cuts and Ejcut	w/ photon cuts and Mjjcut
IHDM1	0.44 (0.56, 1.79)	0.97 (1.21, 3.23)
IHDM2	0.22 (0.28, 0.88)	0.48 (0.59, 1.59)
IHDM3	0.16 (0.21, 0.67)	0.36 (0.45, 1.21)
IHDM4	0.15 (0.19, 0.62)	0.33 (0.41, 1.11)
IHDM5	0.28 (0.35, 1.12)	0.61 (0.76, 2.03)
IHDM6	0.18 (0.23, 0.72)	0.39 (0.49, 1.30)
IHDM7	0.16 (0.21, 0.67)	0.36 (0.45, 1.21)
IHDM8	0.15 (0.19, 0.62)	0.33 (0.41, 1.11)
IHDM9	0.18 (0.23, 0.75)	0.41 (0.50, 1.35)
IHDM10	0.16 (0.20, 0.64)	0.35 (0.43, 1.16)
IHDM11	0.15 (0.19, 0.62)	0.33 (0.41, 1.11)

TABLE XI. Production rates (in fb) at detector-simulation level (after PGS) for $pp \rightarrow jjh \rightarrow jj\gamma\gamma$ for the 2HDM at the LHC-7 (LHC-8, LHC-14). Here $\sigma \cdot B$ denotes $\sigma(pp \rightarrow jjh) \times B(h \rightarrow \gamma\gamma)$. The dijet tag is given in Eqs. (10) and (11) (Ejcut or Mjjcut) and the photon cuts are in Eq. (13).

Model	$\sigma \cdot B$ (fb)	
	w/ photon cuts and Ejcut	w/ photon cuts and Mjjcut
2HDM1	0.17 (0.22, 0.70)	0.38 (0.47, 1.25)
2HDM2	0.41 (0.52, 1.66)	0.90 (1.11, 2.99)
2HDM3	0.44 (0.56, 1.79)	0.97 (1.20, 3.23)
2HDM4	0.45 (0.58, 1.85)	1.00 (1.24, 3.33)
2HDM5	0.12 (0.15, 0.48)	0.26 (0.32, 0.87)
2HDM6	0.24 (0.30, 0.96)	0.52 (0.65, 1.74)
2HDM7	0.15 (0.19, 0.62)	0.33 (0.41, 1.11)
2HDM8	0.09 (0.11, 0.35)	0.19 (0.23, 0.63)
2HDM9	0.29 (0.37, 1.18)	0.64 (0.79, 2.12)
2HDM10	0.15 (0.19, 0.62)	0.33 (0.41, 1.11)

TABLE XII. Production rates (in fb) at detector-simulation level (using PGS) for $pp \rightarrow jjh \rightarrow jj\gamma\gamma$ for selected MSSM and NMSSM benchmark points at the LHC-7 (LHC-8, LHC-14). Here $\sigma \cdot B$ denotes $\sigma(pp \rightarrow jjh) \times B(h \rightarrow \gamma\gamma)$. The dijet tag is given in Eqs. (10) and (11) (Ejcut or Mjcut) and the photon cuts are in Eq. (13).

MSSM BP	$\sigma \cdot B$ (fb)	
	w/ photon cuts and Ejcut	w/ photon cuts and Mjcut
BP1	0.19 (0.28, 0.83)	0.44 (0.57, 1.47)
BP2	0.22 (0.33, 0.97)	0.52 (0.66, 1.76)
BP3	0.29 (0.40, 1.18)	0.63 (0.82, 2.10)
BP4	0.19 (0.28, 0.85)	0.43 (0.56, 1.46)
BP5	0.22 (0.32, 0.92)	0.50 (0.65, 1.65)
BP6	0.27 (0.38, 1.07)	0.61 (0.75, 1.90)
BP7	0.20 (0.26, 0.85)	0.43 (0.53, 1.47)
BP8	0.21 (0.29, 0.85)	0.44 (0.59, 1.48)
BP9	0.22 (0.30, 0.92)	0.49 (0.59, 1.66)